

RESEARCH ARTICLE | JUNE 02 2025

# Free-space and polarization maintaining delivery of terahertz radiation from a quantum cascade laser in a dry dilution refrigerator

M. T. Vaughan ; W. Michailow ; R. Xia ; L. Li ; M. Salih ; H. E. Beere ; D. A. Ritchie ; E. H. Linfield ; A. G. Davies ; J. R. Freeman ; J. E. Cunningham 



Rev. Sci. Instrum. 96, 063901 (2025)

<https://doi.org/10.1063/5.0250844>



## Articles You May Be Interested In

Directed delivery of terahertz frequency radiation from quantum cascade lasers within a dry 3He dilution refrigerator

Rev. Sci. Instrum. (November 2022)

Piezoelectric rotator for studying quantum effects in semiconductor nanostructures at high magnetic fields and low temperatures

Rev. Sci. Instrum. (November 2010)

Integrated Simulation of an Aspheric Lens Combining Injection Moulding Analysis with Ray Tracing

AIP Conf. Proc. (May 2007)

04 June 2025 11:05:30



Review of  
Scientific Instruments  
Special Topics Now Online

[Learn More](#)

# Free-space and polarization maintaining delivery of terahertz radiation from a quantum cascade laser in a dry dilution refrigerator

Cite as: Rev. Sci. Instrum. 96, 063901 (2025); doi: 10.1063/5.0250844

Submitted: 27 November 2024 • Accepted: 30 April 2025 •

Published Online: 2 June 2025



View Online



Export Citation



CrossMark

M. T. Vaughan,<sup>1,a)</sup> W. Michailow,<sup>2</sup> R. Xia,<sup>2</sup> L. Li,<sup>1</sup> M. Salih,<sup>1</sup> H. E. Beere,<sup>2</sup> D. A. Ritchie,<sup>2</sup> E. H. Linfield,<sup>1</sup> A. G. Davies,<sup>1</sup> J. R. Freeman,<sup>1</sup> and J. E. Cunningham<sup>1,b)</sup>

## AFFILIATIONS

<sup>1</sup>School of Electronic and Electrical Engineering, University of Leeds, Leeds, West Yorkshire LS2 9JT, United Kingdom

<sup>2</sup>Cavendish Laboratory, University of Cambridge, Cambridge CB3 0HE, United Kingdom

<sup>a)</sup>Author to whom correspondence should be addressed: [M.T.Vaughan@leeds.ac.uk](mailto:M.T.Vaughan@leeds.ac.uk)

<sup>b)</sup>[J.E.Cunningham@leeds.ac.uk](mailto:J.E.Cunningham@leeds.ac.uk)

## ABSTRACT

We demonstrate a free-space terahertz (THz) optical system inside a dry dilution refrigerator that allows us to direct polarized THz radiation from a quantum cascade laser (QCL) to a sample held at a base temperature of 28 mK. The sample temperature increases to 47 mK for an average applied 2.6 THz QCL power of 27  $\mu$ W at a 10% duty cycle, as determined by calibrated thermometry. We also demonstrate that polarization is maintained using a polarization-sensitive bowtie-antenna-patterned photo-electric tunable step device and, additionally, that the polarization can be adjusted using a set of quartz waveplates in a filter wheel. With this work we introduce the ability to measure materials under polarized THz radiation at previously unreachable millikelvin temperatures.

© 2025 Author(s). All article content, except where otherwise noted, is licensed under a Creative Commons Attribution (CC BY) license (<https://creativecommons.org/licenses/by/4.0/>). <https://doi.org/10.1063/5.0250844>

## I. INTRODUCTION

Terahertz (THz) radiation has a photon energy commensurate with the intrinsic energy scales of many condensed matter systems of contemporary interest, including topological insulators, antiferromagnets, and two-dimensional electron gases.<sup>1–5</sup> It is often the case that the quantum properties of these systems either emerge or become readily observable only at very low temperatures (below 300 mK, for example). A significant difficulty in integrating THz sources directly into the sample space of sub-300 mK cryostats is the limited cooling power available there (typically less than 1 mW below 300 mK), which is incompatible with the heat generated by many THz sources [including quantum cascade lasers (QCLs)], which can be as large as 10 W.

Our previous work developed a system to couple THz radiation from a QCL into the <300 mK sample space environment of a dilution refrigerator by mounting the QCL on a higher temperature stage and using copper hollow metal waveguides (HMWG)

with appropriate thermal decoupling linkages to direct its output to the sample space.<sup>6</sup> We achieved a base temperature of 114 mK before illumination and 160 mK during sample illumination from a THz QCL using this scheme. While the system we introduced met its aims, one drawback was the highly multimode/light pipe system of the HMWG employed, which did not preserve polarization (or, therefore, allow for its systematic control). Being able to define and control the incident polarization would significantly enhance the utility of low temperature THz excitation schemes and expand their potential applications.

While polarization maintaining single-mode waveguides are available,<sup>7–10</sup> they suffer from being bulky, rigid, difficult to align, and having higher loss (than our multimode HMWG). In addition, since some are constructed from dielectric materials, they may be incompatible with cryogenic temperature operation owing to either outgassing in the refrigerator's vacuum environment or cracking on repeat thermal cycling. Here, we demonstrate an alternative scheme for THz excitation by a QCL within a dilution refrigerator making

use of free-space THz optics within the refrigerator and show how polarization of the resulting illumination can be adjusted alongside maintaining low temperature operation.

### A. QCL source and polarization control

We employ a THz QCL with a bound-to-continuum active region using a single metal waveguide design for optical confinement, operating at a center frequency of 2.6 THz, as determined by FTIR spectrometry with a spectral range of 2.5–2.75 THz<sup>21</sup> (see the [supplementary material](#)). The QCL was mounted on a copper heat sink on the pulse tube first stage (PT1) of the (Oxford Instruments Triton) dry dilution refrigerator [Fig. 1(a)]. This stage is held at 48 K with 40 W of cooling power available. This is sufficient cooling power that the refrigerator’s basic operation is unaffected by the additional heat dissipation by the QCL, which was limited to an average of ~2 W by employing pulse mode operation (0.441 ms duration current pulses at a duty cycle of 10% at a frequency of 227 Hz).

Integrating the QCL inside the dilution refrigerator eliminates the need for a second cryostat and the associated logistical challenges

associated with operating two cryostats, including the issue of passing THz from one to another without adding excessive heat loads to either from ambient heat or high losses from windows into the vacuum chamber.

The QCL emits a diverging THz beam that was collimated close to its emission facet using a ZEONEX (E48R) 12 mm diameter lens with a focal length of 9 mm. Quarter waveplates (QWPs) designed for the QCL frequency (2.6 THz) were made from x-cut quartz, with a diameter of 8 mm and a thickness of 0.652 mm. These were used to obtain circularly polarized light in either handedness from the predominantly linearly polarized QCL output.<sup>11</sup> Two QWPs were also stacked together to form a half waveplate (HWP). The waveplates were mounted in a six-position filter wheel through which the collimated THz beam passed. The QCL emits mainly linear TM-polarized THz radiation with the electric field perpendicular to the plane of the semiconductor layers [Fig. 1(b)]; by rotating a wire grid polarizer in front of the THz QCL in a separate experiment, we verified a linear polarization excitation ratio in orthogonal directions (the QCL growth direction and along the ridge width) of  $1:21.8 \pm 0.6$ .

The six filter wheel positions shown in Fig. 1(b) contain the following optical elements: (1) a “Quartz Ref.” position containing a QWP with its fast axis aligned with the QCL polarization axis; this should not induce a change in THz polarization with respect to the QCL output but instead act as a reference for other positions; (2) a “half waveplate” position containing a quartz HWP that rotates the polarization by 90°; (3) “Left handed” and (4) “Right handed” positions containing quartz QWPs designed to produce left-handed and right-handed circular polarizations, respectively; (5) a “blocked” position covered by metal foil; and (6) an “open” position allowing the THz beam to pass through unimpeded. The filter wheel was rotated by a stepper motor compatible with both vacuum and low-temperatures.<sup>12</sup>

### B. Thermal management

There are three nested layers of thermal radiation shields attached to and cooled by the pulse tube first stage (PT1), pulse tube second stage (PT2), and still stage. Each shield blocks thermal radiation from the shield surrounding it so that blackbody background radiation is progressively removed at lower positions within the refrigerator. We can approximate the thermal power leaking through any gap in the thermal shields using the Stefan-Boltzmann law. For a given temperature difference ( $T_{hot}$ ,  $T_{cold}$ ) and hole size (area  $A$ ), the power ( $P$ ) is given by  $P = \sigma \epsilon A (T_{hot}^4 - T_{cold}^4)$ ; here, the emissivity ( $\epsilon$ ) can be assumed to be 1, and  $\sigma$  is the Stefan-Boltzmann constant. Therefore, to minimize heat leaks into colder stages, as small a hole as possible should be formed between stages while still allowing the passage of the THz beam, noting that by far the greatest heating effect arises from heat leaking from the hottest stages.

We chose to employ a pair of lenses to focus the THz beam through a 5 mm diameter hole in the PT2 radiation shield and then collimate it on the far side. A copper foil shield was placed around the upper lens to help shield the hole from stray thermal radiation. For the still stage, a High Density Polyethylene (HDPE) filter was found to be sufficient since the power of <4 K blackbody radiation has minimal effect on sample heating. This method satisfies two major constraints for the successful integration of free-space

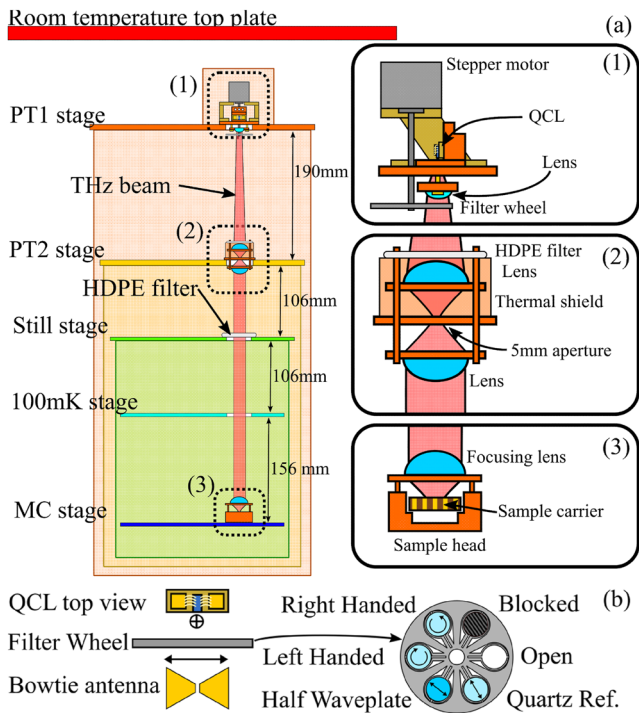


**FIG. 1.** (a) Free-space optical path extends from the THz QCL on the PT1 stage to the sample, which is held on the mixing chamber (MC) stage. The divergent THz beam from the QCL is collimated by a lens (1). The double lens assembly shields the lower stages from thermal radiation, along with 2 HDPE inserts on the PT2 stage and still stage (2). Finally, the THz is received by the sample lens, focusing the THz onto the device (3). Three layers of thermal radiation shielding are shown, colored according to their appropriate stage. See the [supplementary material](#) for photographs of each component. (b) The filter wheel contains several quarter waveplates and a half waveplate, as well as one empty slot and another fully blocked, as indicated. The filter wheel is rotated by a stepper motor. The relative orientations of the QCL polarization (out of the page) and bowtie antenna (left to right) are depicted as orthogonal.

04 June 2025 11:05:30

optics by simultaneously minimizing heat leakage while allowing optical access with a reasonably wide THz beam. The lenses used were 25 mm in diameter with a 17.5 mm focal length and made from ZEONEX E48R polymer. We note that the refractive index for ZEONEX E48R is very similar at optical and THz frequencies (1.515 and 1.530, respectively<sup>13</sup>). Importantly, this also permitted initial alignment at room temperature using visible light.

ZEONEX E48R is effective at blocking thermal IR radiation; we estimate a 2-mm-thick piece of ZEONEX blocks 85% of 290 K blackbody radiation while transmitting 75% of radiation at our 2.6 THz QCL frequency.<sup>14,15</sup> To provide additional blocking of IR radiation, we used 2 mm thick HDPE inserts as filters; we estimate that these also block ~85% of the IR blackbody radiation while transmitting 80% of the THz radiation.<sup>16</sup> Two HDPE inserts were placed in positions expected to be most effective at blocking thermal radiation, one in front of the lens pair assembly and the other on the PT2 stage [Fig. 1(a)].

### C. Sample holder

Our sample holder consists of a copper mount supporting a focusing lens and an LCC20 socket allowing electrical connection to the sample, which was mounted in a standard LCC20 chip carrier. The focusing lens was another E48R ZEONEX lens (12 mm diameter, 9 mm focal length) used to focus THz radiation from the collimated THz beam onto the chip surface. The test device used here was a photo-electric tuneable-step (PETS) THz detector with an integrated bowtie antenna.<sup>4</sup> In these devices, a potential step is created within the plane of a 2D electron system by biasing two gates with a nanoscale gap between them. Upon exposure to terahertz radiation, the field confined between the gates gives rise to a photocurrent due to the in-plane photoelectric effect. A bowtie antenna is used to increase coupling to the far-field THz radiation. The antenna is most sensitive to electric fields along its long axis. As such, we expect a “figure-8” response as a function of polarization angle for incoming linearly polarized THz radiation. The bowtie should be equally sensitive to left- and right-handed circularly polarized THz radiation.

## II. BENCHTOP MEASUREMENTS OF SUBASSEMBLIES

Alignment of the complete optical THz beam path was achieved by starting with alignment of each subassembly separately on an optical benchtop, allowing us to optimize alignment and characterize component performance simultaneously (Fig. 2) before integration with the dilution refrigerator. A small 50 K cryocooler was used to cool the THz QCL during benchtop alignment since it allowed fast alignment and adjustments. The space between subassemblies should predominantly be a collimated THz beam along a straight vertical axis from the QCL source on the PT1 stage through to the sample on the mixing chamber stage and, as such, subassemblies were optimized to either emit (via a QCL + collimating lens) or maintain (via a lens pair) the collimated THz beam.

### A. Collimating the QCL emission

Starting with the THz QCL (without the stepper motor or filter wheel), the collimating lens and QCL were carefully positioned

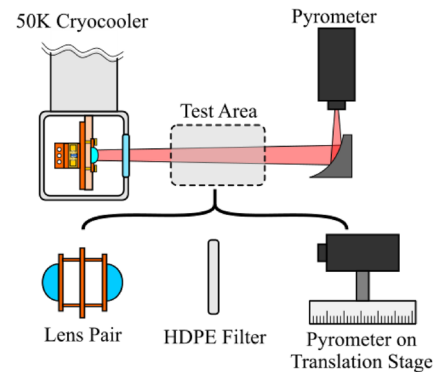


**FIG. 2.** Benchtop method for aligning subassemblies and characterizing the losses of each component. The QCL and collimating lens are placed inside a 50 K cryocooler with HDPE windows. The THz beam was then detected using a parabolic mirror and pyrometer. Between these is the “Test Area,” a cross section used for measuring the QCL beam profile and characterizing of the other subassemblies.

such that the THz radiation diverging from the QCL facet was collimated by the ZEONEX lens. Initial alignment was performed using white light and by moving the QCL until the emitting ridge was in focus.

The QCL with collimating lens was then loaded into a 50 K cryocooler to simulate conditions inside the dilution refrigerator at the PT1 stage it would be mounted to later. Using this setup, the THz beam width was measured using a pyrometer on a translation stage (Fig. 2). The THz beam profile was deliberately optimized to have a slight divergence to mitigate against slight pointing errors. In addition, the beam diameter for this THz beam profile provided a better match to the lens diameter of the lens pair [Fig. 1(a.2)], though at the cost of a slightly lower transmitted power since some of the outer perimeter beam profile was cut off. The final beam divergence from the QCL collimating lens was measured to be  $7.2^\circ$ , with a FWHM beam diameter of 20.5 mm at a distance of 210 mm from the QCL, which is the approximate distance (190 mm) and lens diameter (25 mm) of the lens pair subassembly, respectively.

### B. Lens pair subassembly and HDPE filters

Using the slightly divergent beam and an off-axis parabolic mirror to focus the THz beam onto a pyrometer, the lens pair assembly was iteratively optimized by changing the lens spacing to adjust power transmission (Fig. 2), resulting in an optimized alignment at room temperature with a THz transmission of ~20%. Most of the loss was attributed to absorption within the two thick ZEONEX E48R polymer lenses. The THz transmission efficiency of the HDPE filter in front of the lens pair assembly was then measured to be 74%.

Upon cooling to cryogenic temperatures, the distance between the pair of ZEONEX lenses was estimated to shrink by 0.13 mm as the brass metal contracts,<sup>17</sup> which results in slight but unavoidable deviation from optimal alignment. Using a thin lens approximation, we calculate that the added beam divergence to be only around  $0.31^\circ$ , which is much smaller than the beam divergence after the QCL collimation lens mentioned earlier. As such, we do not expect thermal contraction in this location to impact alignment significantly or result in substantial additional power loss.

### C. Sample lens

The final optical component was a lens placed immediately above the PETS device on the Mixing Chamber (MC) stage [Fig. 1(a.3)]. This collects the THz radiation and focuses it onto the center of the PETS device. The alignment of this lens was performed at room temperature, using the magnified image of the device viewed from the lens position. In these measurements the PETS device was placed slightly closer than the focal length of the lens in order to increase the spot size, thus ensuring that its sensitive detection region was fully illuminated. As such, there was a deliberate trade-off of slightly lower power density for greater certainty of THz detection.

### D. Final installation of subassemblies and global alignment

Finally, after each subassembly was individually aligned, each component was placed inside the dilution refrigerator, and a “global” alignment was then undertaken of the subassemblies relative to each other. The horizontal plates that make up each stage of the fridge were known to be reasonably parallel, with only minor corrections needed. Thin metal shims inserted under the edges of the subassemblies were used to tilt the subassemblies to remove residual optics misalignment as needed.

By placing an orange LED in the sample holder, any residual alignment errors could be assessed. The LED illuminated the THz optical path “backward” from the sample position so that once the light was seen to reach the QCL ridge, the complete path could be seen to be aligned. Typically, we found that the lens pair assembly was the only component that needed minor shimming to align the optical path at this stage, after which the HDPE filters could be installed. Since these filters are flat and only 2 mm thick, we found that they did not significantly deflect the THz beam.

## III. EVALUATING SYSTEM PERFORMANCE

With all components installed in the dilution refrigerator, the MC stage reached a base temperature of 27 mK. By comparison, the same system achieved 114 mK in our previous work with THz HMWGs installed;<sup>6</sup> our efforts here thus demonstrate a significant reduction in residual thermal loading compared to that arrangement.

Next, we verified how much THz power was reaching the sample position on the MC stage. We calibrated the MC thermometer with a known thermal loading (via the Joule heating of a resistor) to determine the absorbed THz power. Figure 3 shows the calibrated thermometer response as a function of QCL drive current, together with the estimated THz power absorbed at the MC stage. The maximum average power absorbed at the MC stage was  $27.4 \mu\text{W}$  for a 1600 mA QCL drive current with a 10% duty cycle, with the MC stage then maintaining a temperature of  $\sim 47$  mK. The maximum power received at the MC closely matches that of our benchtop QCL characterization.

We next found the optimal bias voltage for THz detection in our PETS antenna by sweeping a 2D map of both the wide and narrow gate bias, which showed the typical features of both positive and negative responses localized along the edges of where the conducting channel starts to open (narrow gate  $> -0.11$  V and wide

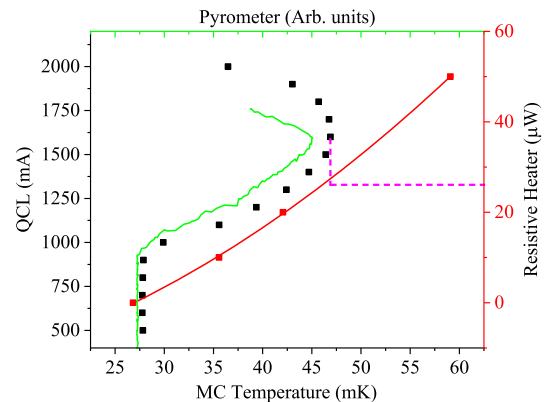


**FIG. 3.** Calibrated thermometry of the MC stage compared to the heating from THz radiation. A parabolic calibration curve is fitted to the resistive heating data (red line). The largest THz heating effect occurs at a QCL bias of 1600 mA, increasing the temperature from 27.8 to 46.9 mK, corresponding to a power of  $27.4 \mu\text{W}$ . The dashed purple line is a guide to the eye for calculations of the THz signal from the calibration curve. The green curve is a benchtop power measurement using a pyrometer. The filter wheel was placed in the open position for these measurements. The dominant frequency at peak THz power was 2.6 THz (see the supplementary material).

gate  $> -0.23$  V).<sup>4</sup> The photovoltage was measured with a lock-in amplifier and using the QCL pulsed frequency (226 Hz) as reference. The photovoltage changes polarity as it changes sign when the direction of the potential step is reversed (Fig. 4). The optimal gate biases for the THz detector occur when the wide and narrow gates are biased at  $-0.205$  and  $-0.115$  V, respectively. The right-handed filter position was used for this since it happened to give the largest response.

Once the optimum gate biases were chosen for the detector, the response to the terahertz radiation could be investigated. Figure 5 shows the photovoltage of the PETS bowtie antenna for different

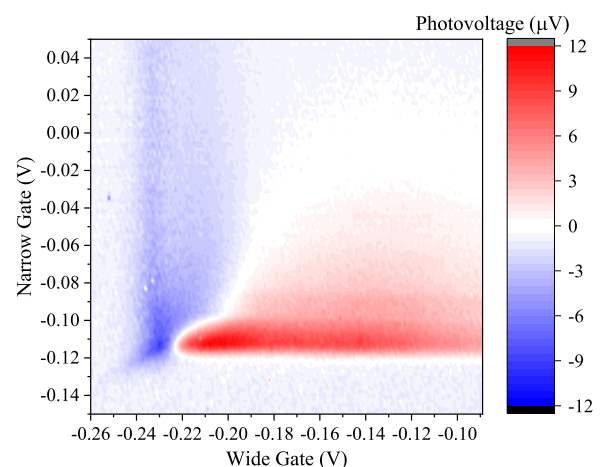


**FIG. 4.** 2D plot of the photovoltage from a PETS device. The filter position was “Right handed” polarization with 1600 mA QCL bias and a 10% duty cycle, found to give the largest response.

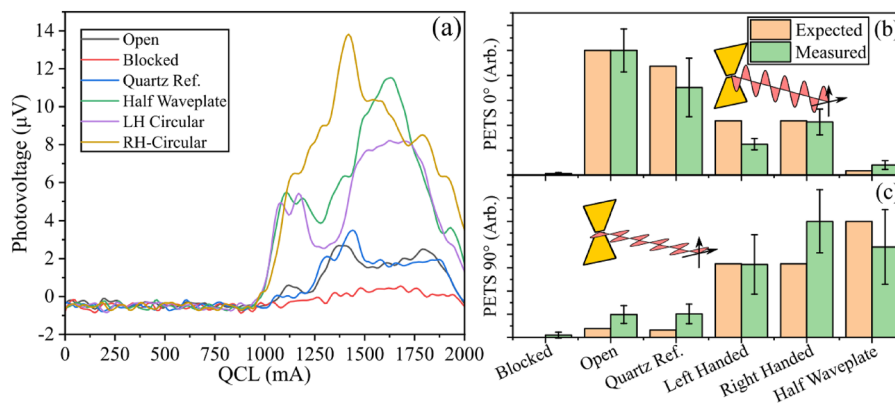


**FIG. 5.** (a) Photovoltage from the PETS detector as a function of QCL current for each of the filter positions with the final free-space optical path at 30 mK. By taking the mean and standard deviation between 1300 and 1800 mA, we plot a bar chart to compare the expected photovoltage with the measured response (b) and (c). The small inset diagram in (b) and (c) represents the unmodified (“open”) polarization orientations. (c) Bottom bar chart is the final free-space optical path taken from Fig. 5(a). (b) In comparison, the top bar chart (PETS 0°) is from early in the free-space optics development, showing the predicted and measured photovoltage when the QCL polarization and bowtie antenna are aligned.

QCL bias currents and for different polarizing filter wheel positions at the optimal gate bias for THz detection. As expected from the orientation of the PETS device with respect to the measured polarization of the THz QCL, the “Open” filter wheel position produces only a very small THz photovoltage since the corresponding polarization arriving at the sample is perpendicular to the long axis of the bowtie antenna and, therefore, unable to excite a large signal. Similarly, the “Quartz Ref.” position (where the polarization is also unchanged) also shows a low photovoltage. The “blocked” filter position further reduces the observed photovoltage down to a minimal level associated with residual background signal in the PETS detector.

When any of the three polarization-modifying quartz filter positions were used (“Half Waveplate,” “Right Handed circular,” or “Left Handed”), however, the measured response from the sample was found to be much larger than either “Open” or “Quartz Ref.” filter positions. This, along with the former results, demonstrates directly that the polarization of the THz radiation from the QCL can be adjusted by the use of appropriate quartz waveplates, as they act to increase the component of the electric field parallel to the bowtie antenna (which is the axis of the PETS device most sensitive to THz radiation).

We note that the repeatable noise seen in Fig. 5(a) during QCL operation could potentially result from a speckle pattern formed on the surface of the device owing to interference from random imperfections in the free-space optical path. Either changes to the QCL THz frequency (such as by using different current bias) or small changes in path length from different filter positions would slightly change the speckle pattern on the surface of the sample, giving a fluctuating response as maxima and minima move over a sensitive region of a detector. We also note, therefore, that a change in QCL frequency could result in a change in the PETS detector response owing to Fabry–Pérot effects within the substrate of the PETS detector.<sup>19</sup>

To better compare the photovoltage for each filter position, the mean and standard deviation were taken in the range of QCL currents from 1300 to 1800 mA and compared with the expected response [Figs. 5(b) and 5(c)]. The expected response was estimated by assuming 75% transmission for a 1 mm thick quartz filter, that the QCL radiation is 95% linearly polarized as estimated from the measured 1:21.8 ± 0.6 extinction ratio mentioned earlier, and that the PETS bowtie antenna is only sensitive to electric fields along its length, with no dependence on handedness.

For completeness, in Fig. 5(b), we also include measurements from an earlier experiment made during development of the free-space optical path in which the sample was located on the PT2 stage at 3.5 K.<sup>18</sup> As indicated, in this configuration the PETS bowtie antenna was rotated 90° with the antenna aligned with the QCL polarization. In this configuration, the expected photovoltage was then greatest in the “open” and “quartz ref.” positions, with a minimal response expected from the “half waveplate” position. The measured photovoltage again closely follows the expected trend, providing further evidence that the free-space optics maintain polarization and that the filter can be used to adjust this polarization.

It was anticipated that the “Half Waveplate” position would give the largest photovoltage, with the two QWPs giving ~50% of that maximum. However, in Fig. 5(c), it can be seen that the largest response is actually obtained from the “Right handed” filter position. It is also unclear why there is this small difference between the “Right Handed” and “Left Handed” polarization filter positions since the symmetric bowtie antenna should be insensitive to handedness. One possibility is that the filter positions are not perfectly set at 45°; deviations from 45° would reduce the photovoltage for the half waveplate and QWPs.

It is clear, however, that the filter wheel largely has the intended effect on polarization, given that each measured photovoltage lies within, or close to, the error bars [Figs. 5(b) and 5(c)]. Future work

will concentrate on further enhancing the purity of the polarization obtained by adjustments to the filter wheel and the waveplate used.

#### IV. CONCLUSION

Through careful management of thermal loads, mitigating issues with free-space optics, and having a clear understanding of the requirements needed to achieve useful THz power, we have built a free-space system that can be used to illuminate materials or devices with THz radiation from a QCL inside a dilution refrigerator. We also demonstrated that polarization is maintained and can be altered using quartz waveplates. The sample temperatures are maintained at <50 mK throughout, representing a substantial improvement over our previous work using HMWG, which achieved 160 mK under THz illumination. We anticipate our technique will be useful in the study of a wide range of condensed matter systems.

In general, magnetic fields offer a useful tool for breaking time-reversal symmetry in many condensed matter systems, resulting in polarization dependence on illumination. Future improvements to the system will therefore include extending the THz optical path using a pair of 90° reflectors to reach the 12 T magnet bore in our system, which could be particularly useful for probing cyclotron resonance modes with circularly polarized THz light, for example. Another future improvement could be demonstration of detection by self-mixing using the THz-QCL,<sup>20</sup> enabled by the polarization-maintaining free-space beam path now demonstrated.

#### SUPPLEMENTARY MATERIAL

The [supplementary material](#) contains the QCL THz spectrum at 50 K as well as photos on the final freespace optical setup as shown in [Fig. 1\(a\)](#).

#### ACKNOWLEDGMENTS

We would like to acknowledge our funders EPSRC through Grant Nos. EP/V001914/1, EP/W028921/1, EP/V047914/1, and EP/V004743/1, and Horizon Europe via the grant “Extreme-IR” Grant No. 964735.

#### AUTHOR DECLARATIONS

##### Conflict of Interest

The authors have no conflicts to disclose.

#### Author Contributions

**M. Vaughan:** Conceptualization (equal); Data curation (equal); Formal analysis (equal); Investigation (equal); Methodology (equal); Resources (equal); Software (equal); Writing – original draft (equal); Writing – review & editing (equal). **W. Michailow:** Resources (equal); Supervision (equal); Writing – review & editing (equal). **R. Xia:** Resources (equal). **L. Li:** Resources (equal). **M. Salih:** Resources (equal). **H. Beere:** Funding acquisition (equal); Supervision (equal). **D. A. Ritchie:** Supervision (equal). **E. H. Linfield:** Funding acquisition (equal); Supervision (equal). **A. G. Davies:** Funding acquisition

(equal); Supervision (equal); Writing – review & editing (equal). **J. R. Freeman:** Funding acquisition (equal); Supervision (equal); Writing – review & editing (equal). **J. E. Cunningham:** Funding acquisition (equal); Supervision (equal); Writing – original draft (equal); Writing – review & editing (equal).

#### DATA AVAILABILITY

Data for this work are openly available and stored by the University of Leeds data repository.<sup>21</sup>

#### REFERENCES

- J. Li, C. B. Wilson, R. Cheng, M. Lohmann, M. Kavand, W. Yuan, M. Aldosary, N. Agladze, P. Wei, M. S. Sherwin, and J. Shi, “Spin current from sub-terahertz-generated antiferromagnetic magnons,” *Nature* **578**, 70 (2020).
- H. Plank, J. Pernul, S. Gebert, S. N. Danilov, J. König-Otto, S. Winnerl, M. Lanius, J. Kampmeier, G. Mussler, I. Aguilera, D. Grützmacher, and S. D. Ganichev, “Infrared/terahertz spectra of the photogalvanic effect in (Bi,Sb)Te based three-dimensional topological insulators,” *Phys. Rev. Mater.* **2**(2), 024202 (2018).
- C. S. Knox, M. T. Vaughan, A. D. Burnett, M. Ali, S. Sasaki, E. H. Linfield, A. G. Davies, and J. R. Freeman, “Effects of structural ordering on infrared active vibrations within Bi<sub>2</sub>(Te<sub>(1-x)</sub>Se<sub>x</sub>)<sub>3</sub>,” *Phys. Rev. B* **106**, 245203 (2022).
- W. Michailow, P. Spencer, N. W. Almond, S. J. Kindness, R. Wallis, T. A. Mitchell, R. Degl’Innocenti, S. A. Mikhailov, H. E. Beere, and D. A. Ritchie, “An in-plane photoelectric effect in two-dimensional electron systems for terahertz detection,” *Sci. Adv.* **8**(15), eabi8398 (2022).
- D. M. Mittleman, “Frontiers in terahertz sources and plasmonics,” *Nat. Photonics* **7**(9), 666–669 (2013).
- M. Vaughan, W. Michailow, M. Tan, M. Salih, L. Li, H. Beere, D. A. Ritchie, E. H. Linfield, A. G. Davies, and J. E. Cunningham, “Enhanced delivery and detection of terahertz frequency radiation from a quantum cascade laser within dilution refrigerator,” *J. Low Temp. Phys.* **213**(5–6), 306–316 (2023).
- G. Xie, Y. Zhong, G. Li, C. She, X. Lu, F. Yue, S. Liu, C. Jing, Y. Cheng, and J. Chu, “300 GHz bending transmission of silver/polypropylene hollow terahertz waveguide,” *Results Phys.* **19**, 103534 (2020).
- M. Navarro-Cía, M. S. Vitiello, C. M. Bledt, J. E. Melzer, J. A. Harrington, and O. Mitrofanov, “Terahertz wave transmission in flexible polystyrene-lined hollow metallic waveguides for the 2.5–5 THz band,” *Opt. Express* **21**(20), 23748 (2013).
- G. Gallot, S. P. Jamison, R. W. McGowan, and D. Grischkowsky, “Terahertz waveguides,” *J. Opt. Soc. Am. B* **17**(5), 851 (2000).
- C. D. Nordquist, M. C. Wanke, A. M. Rowen, C. L. Arrington, M. Lee, and A. D. Grine, “Design, fabrication, and characterization of metal micromachined rectangular waveguides at 3 THz,” in *2008 IEEE Antennas and Propagation Society International Symposium* (IEEE, San Diego, CA, 2008), pp. 1–4.
- G. Liang, T. Liu, and Q. J. Wang, “Recent developments of terahertz quantum cascade lasers,” *IEEE J. Sel. Top. Quantum Electron.* **23**(4), 1200118 (2017).
- Lewvac, M-D35.1, 2024, <https://www.lewvac.co.uk/product/uhv-vacuum-stepper-motors/>.
- C. Brückner, B. Pradarutti, R. Müller, S. Riehemann, G. Notni, and A. Tünnermann, “Design and evaluation of a THz time domain imaging system using standard optical design software,” *Appl. Opt.* **47**, 4994 (2008).
- See [https://www.tydexoptics.com/pdf/THz\\_Materials.pdf](https://www.tydexoptics.com/pdf/THz_Materials.pdf) for information on transmission spectrum for several optical materials at THz frequencies.
- E. J. Wollack, K. L. Denis, A. Barlis, M.-P. Chang, A. S. Kutyrev, K. H. Miller, and P. C. Nagler, “Far-infrared properties of cyclic olefin copolymer,” *Opt. Lett.* **45**(3), 780 (2020).
- C. Balocco, L. Mercatelli, N. Azzali, M. Meucci, and G. Grazzini, “Experimental transmittance of polyethylene films in the solar and infrared wavelengths,” *Sol. Energy* **165**, 199–205 (2018).
- E. D. Marquardt, J. P. Le, and R. Radebaugh, “Cryogenic material properties database,” *Cryocoolers* **11**, 681–687 (2002).

<sup>18</sup>M. Vaughan, W. Michailow, R. Xia, M. Salih, L. Li, H. Beere, D. Ritchie, E. Linfield, G. Davies, J. Freeman, and J. Cunningham, “Developing free-space and polarization control of THz QCL radiation inside a dry dilution refrigerator,” in *2024 49th International Conference on Infrared, Millimeter, and Terahertz Waves (IRMMW-THz)* (IEEE, 2024).

<sup>19</sup>R. Chen, R. Xia, J. Griffiths, H. E. Beere, D. A. Ritchie, and W. Michailow, “Photoelectric tunable-step terahertz detectors: A study on optimal antenna parameters, speed, and temperature performance,” *Nanophotonics* **13**, 1917 (2024).

<sup>20</sup>A. Valavanis, P. Dean, Y. L. Lim, R. Alhathlool, M. Nikolic, R. Kliese, S. P. Khanna, D. Indjin, S. J. Wilson, A. D. Rakić, E. H. Linfield, and G. Davies, “Self-mixing interferometry with terahertz quantum cascade lasers,” *IEEE Sens. J.* **13**(1), 37–43 (2013).

<sup>21</sup>M. Vaughan, W. Michailow, R. Xia, M. Salih, L. Li, H. Beere, D. Ritchie, E. Linfield, G. Davies, J. Freeman, and J. Cunningham (2025), “Dataset associated with ‘Free-space and polarisation maintaining delivery of terahertz radiation from a quantum cascade laser in a dry dilution refrigerator,’” University of Leeds. <https://doi.org/10.5518/1686>